



Audio Engineering Society

Convention Paper

Presented at the 131st Convention
2011 October 20–23 New York, NY, USA

This Convention paper was selected based on a submitted abstract and 750-word precis that have been peer reviewed by at least two qualified anonymous reviewers. The complete manuscript was not peer reviewed. This convention paper has been reproduced from the author's advance manuscript without editing, corrections, or consideration by the Review Board. The AES takes no responsibility for the contents. Additional papers may be obtained by sending request and remittance to Audio Engineering Society, 60 East 42nd Street, New York, New York 10165-2520, USA; also see www.aes.org. All rights reserved. Reproduction of this paper, or any portion thereof, is not permitted without direct permission from the Journal of the Audio Engineering Society.

An approach to small size direct radiation transducers with high SPL

Martínez, J.¹, Segovia, E.², Ramis, J.³, Espí, A.¹, Carbajo, J.³

¹ Acústica Beyma, S.L., Moncada, Valencia, 46113, Spain
j.martinez@beyma.com, alejandro.espi@beyma.com

² Dpto. Ingeniería de la Construcción, Obras Públicas e Infraestructura Urbana, San Vicent del Raspeig, 03080, Alicante, Spain
enrique.gonzalo@ua.es

³ Dpto. Física, Ingeniería de Sistemas y Teoría de la Señal, San Vicent del Raspeig, 03080, Spain
jramis@ua.es, jesus.carbajo@ua.es

ABSTRACT

This work analyses some of the issues related with small size direct radiation loudspeakers design and aims to achieve high SPL using this kind of loudspeaker. In order to reach it, large diaphragm displacements are needed. Structural dynamic behaviour of the moving assembly must be emphasized. With the aid of a numerical model implemented with finite element theory, it is possible to quantify the influence of changing the number of folds in the suspension (spider), the distance between spiders and the effect of unbalanced forces inherent to the speaker construction. Numerical model predictions are compared with experimental results taking as reference a six inch loudspeaker development.

1. INTRODUCTION

The current trend in PA designs is to minimize the physical dimensions of professional audio systems. This involves the urgent need to build smaller and smaller cabinets, and consequently, small size transducers are required.

Reaching high Sound Pressure Level (SPL) at low frequencies using small size sources involves serious difficulties. These transducers have, obviously, a small effective surface area S_D , so efficiency is low [1], according to direct dependence between both parameters, as shown in (1)

$$\eta_o = \frac{\rho_o}{2\pi c} \frac{(Bl)^2 S_D^2}{R_e M_{MD}^2} \quad (1)$$

As efficiency is low, Sensitivity is also low [2] according to

$$Sens_{1W@1m} = 112.18 + 10 \log \eta_o \quad (2)$$

It is well known that acoustic power radiated by vibrant systems depends on the diaphragm velocity (related with the rated air flow) and the mechanical radiation resistance (real part of mechanical impedance). This impedance is a function of the diaphragm geometry and it controls the acoustic radiation. But, due to limited leeway when designing small size loudspeakers in terms of mechanical radiation impedance, it is necessary to resort to large displacements of the diaphragm. In this context, the optimization of structural dynamic behaviour of the moving assembly must be emphasized. This work analyses some of the issues raised above within the context of developing a six inch direct radiation loudspeaker to reach high SPL.

To accomplish this requirement some problems arise and they are analysed in this paper with the aid of a Finite Element Model (FEM), focusing on the structural dynamic behaviour of the moving assembly. Relying on a numerical model, implemented with finite elements, it is possible to quantify the influence of small changes in the geometry and material characteristics that constitute the moving assembly. A description of the effects of these changes is one of the targets of this work.

Concerning the numerical model implementation, due to the importance of input data information in the simulations, it is described, likewise, the process followed for the spider material characterization (Young modulus and loss factor). This time, the problem was addressed by means of an inverse technique based on reproducing a real experiment – that consists on a double suspension and diaphragm assembly – in order to adjust theoretical data in the finite element model. The variable compared is the resonance frequency, in order to obtain Young Modulus, and the displacements to adjust loss factor.

Finally, a Finite Element Model (FEM) for the loudspeaker moving assembly has been implemented, using the software Ansys®. In this FEM, it was used a SHELL 181 element type which has six degrees of

freedom per node and satisfies the first order shear deformation theory.

Although lower suspension, or spider, is also a limiting factor, it does not affect to the diaphragm displacement as much as upper suspension does. As y-axis displacement depends on fold radius and the number of folds, and surround has considerably less number of folds than spider has, then the surround becomes the most limiting factor for y-axis displacement. Therefore, in order to maximize both y-axis displacement and S_D , the proposal is to eliminate the upper suspension and incorporate a big less stiff double suspension, Fig. 1. The reason to use bigger suspensions is to maximize u_y according to what has just been explained, i.e. to reach very important displacements along the y-axis, whereas the reason to make it double is to minimize u_x , which means no sway displacement in x-axis, avoiding any possibility of friction between the voice coil and the pole piece or top plate.

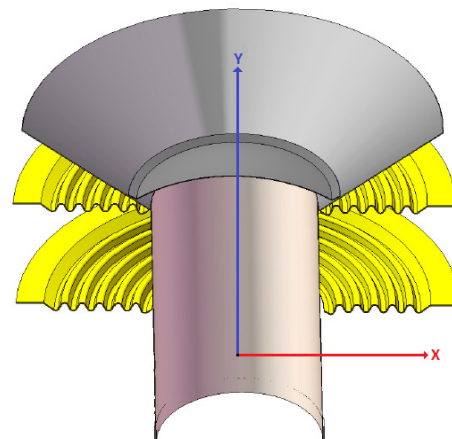


Fig. 1. Moving assembly with double suspension

Regarding magnetic assembly, an underhung geometry, Fig. 2(a), was considered rather than overhung geometry, Fig. 2(b). This is not only due to the fact that very important diaphragm excursions are achieved (high X_{max}) but also it keeps the speaker under linear conditions at higher powers. This geometry will also help to keep third order distortion low [3]. It can be observed in Fig. 2(a) that this configuration requires a shorter voice coil so it will be lighter. Second order distortion also aims to be low according to several conditions exposed in [4] [5].

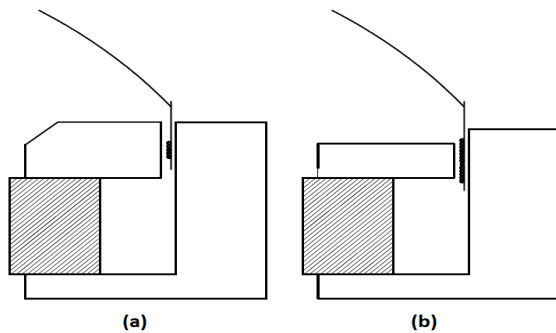


Fig. 2. Gap configurations. (a) Underhung geometry. (b) Overhung geometry

The equivalent numerical model also considers an underhung geometry. Through this numerical model, the influence of changing the number of folds in the suspension, the distance between spiders, symmetrical or asymmetrical orientation for suspensions, and unbalanced forces effect inherent to the speaker construction can be analysed and quantified.

With the use of modal and harmonic analysis tools, the modal base is obtained determining the dynamic behaviour of the moving assembly and also the displacements of every model nodes, being critical in some locations. For example, an excessive displacement in the radial direction of the moving assembly on its lowest part could cause voice coil friction in the gap, which is a risky situation, as it is well known. These data about displacements have been used, for example, to decide the optimal distance between the spiders. Numerical model predictions are compared with experimental results having as reference a six inch loudspeaker development.

2. APPROACH

2.1. Equivalent circuit of an electrodynamic loudspeaker

This work focuses on studying the structural behaviour of moving assembly in the low frequency range, where the displacements are larger. The equivalent circuit, Fig. 3a, depicts the interaction between electrical, mechanical and acoustical elements from mechanical side [6].

In the low frequency region, it is verified that

$$\omega L_E \ll (R_g + R_E) \tag{3}$$

$$\frac{1}{\omega L_E / (Bl)^2} \ll \frac{(Bl)^2}{(R_g + R_E)} \tag{4}$$

With these conditions, the following circuit, Fig. 3b, can be considered as a low frequency approach.

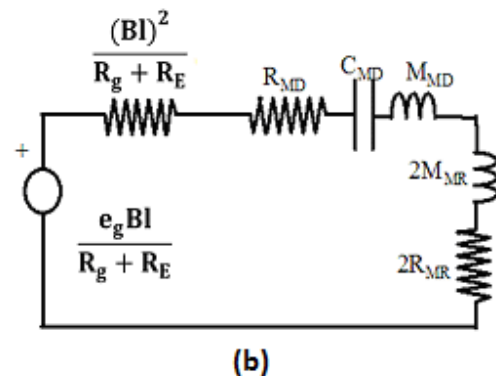
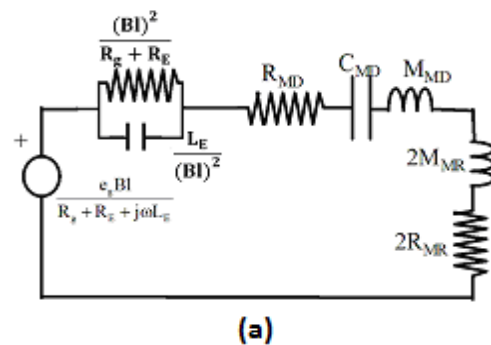


Fig. 3. (a) Mechanical equivalent circuit of an electrodynamic transducer. (b) Equivalent circuit at low frequency.

The mechanical mass of radiation was implemented as an added mass using

$$M_{MR} = \frac{8}{3} \rho_0 a^3 \tag{5}$$

The values of resistors were adjusted using experimented data.

2.2. Finite Element Method (FEM)

FEM is a well extended numerical method for solving numerous physics problems in which differential

equations are involved. Further details related to generic elastic analysis can be found, for example, in [7][8].

To carry out this work, Finite Element Software called *Ansys*© was used. This software includes the global damping matrix composed by the following terms

$$[C] = \alpha[M] + \beta[K] + \left(\frac{\zeta}{\omega}\right)[K] + \sum_{j=1}^M \beta_j [K_j] + \sum_{k=1}^N [C_k] \quad (6)$$

where α is a constant multiplying mass matrix, β is a constant multiplying the stiffness matrix, ζ is damping at a single frequency, β_j is a constant multiplying the stiffness matrix for element type and $[C_k]$ is the damping matrix, which can be defined as an own characteristic for some kind of elements, for example, a spring-like element.

According to introduced constants, which are compatible and cumulative, damping matrix can be defined. With mass, damping and stiffness matrixes, the equation of motion can be written in terms of displacements of the nodes of the elements which constitute the unknowns of the problem.

$$[M]\{\ddot{u}^*\} + [C]\{\dot{u}^*\} + [K]\{u^*\} = \{f^{ext}(t)\} \quad (7)$$

Using the previous expression but considering that systems vibrates freely and without damping and specifying boundary conditions, it is possible to determine the eigenfrequencies and their own modal shapes.

$$[M]\{\ddot{u}^*\} + [K]\{u^*\} = 0 \quad (8)$$

Using a proper base change

$$\{u^*\} = [\Phi]\{\xi^*\} \quad (9)$$

and operating, it is possible to reach, for every i-mode,

$$\ddot{\xi}_i + (\alpha + \beta\omega_i^2)\dot{\xi}_i + \omega_i^2 \xi_i = \frac{\{\phi_i\}^T \{f^{ext}(t)\}}{M_i} \quad (10)$$

It must be noticed that: 1) The two latter terms of Eq. (6) were not considered here and 2) $\{\Phi_i\}$ is normalized with $M_i = 1$

Therefore, for harmonic analysis, participation factor of i-mode can be defined as

$$FP_i = \{\phi_i\}^T \{f_{Max}^{ext}\} \quad (11)$$

3. NUMERICAL MODEL

3.1. Adjusting the model

The most important parameters are suspension material Young modulus and the global system loss factor.

Suspension material Young modulus was obtained using an inverse method. An experimental driver with double suspension and without membrane was built, Fig. 4. Since mass can be easily obtained, the only task is to adjust the numerical model to the experimental driver by matching the resonant frequency of the numerical model with the one obtained experimentally with the impedance curve, Fig. 5.

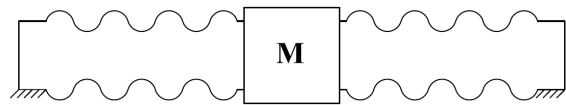


Fig. 4. Experimental driver built to determine suspension material Young modulus.

The procedure to determine the global system loss factor was to adjust diaphragm displacement to a Single Degree Of Freedom (SDOF) system. This time, the numerical model and the experimental driver moving assembly includes all the components.

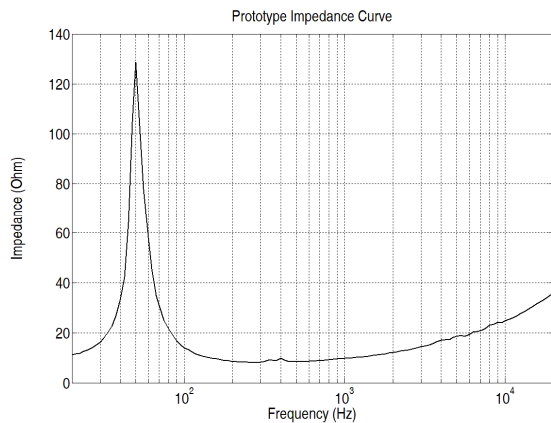


Fig. 5. Electric impedance curve of the experimental driver used to calibrate the numerical model and obtain suspension material Young modulus

Fig. 6 shows experimental diaphragm displacement measurements obtained using Klippel Analyzer system [9] for input voltages of 10, 15 and 20 V.

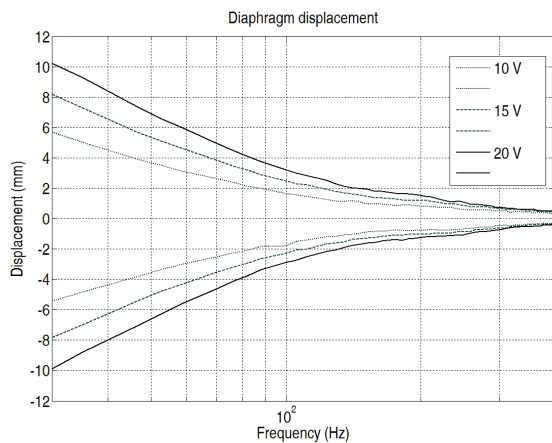


Fig. 6. Diaphragm displacement measurements obtained using Klippel Analyzer system.

SDOF system can be perfectly adjusted by choosing the proper loss factor by fixing α and β parameters of matrix [C]. Then, numerical and experimental results match totally.

Fig. 7 shows a comparison between three different situations: experimental measurements, theoretical simulation with $\beta=0$ and theoretical simulation with $\beta \neq 0$. Since both theoretical simulations are equal, results presented hereafter are considering $\beta=0$.

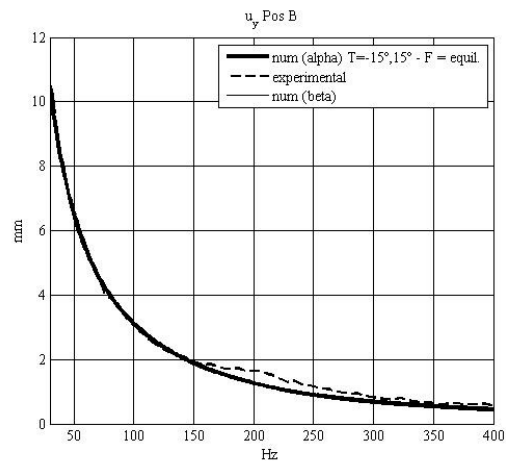


Fig. 7. Comparison between diaphragm displacements obtained with numerical model ($\beta=0$ and $\beta \neq 0$) and experimentally.

3.2. THE MODELS

With the purpose of modelling as many situations as possible, several variables were parameterized. Taking as reference the moving assembly shown in Fig. 8, the influence of number of folds was analysed, as well as the distance between suspensions, symmetrical or asymmetrical configuration for suspensions, Fig. 9, and lead wires position.

The total mass of moving assembly is 24g, which includes the mechanical mass of radiation. Physical dimensions are depicted in Fig. 8.

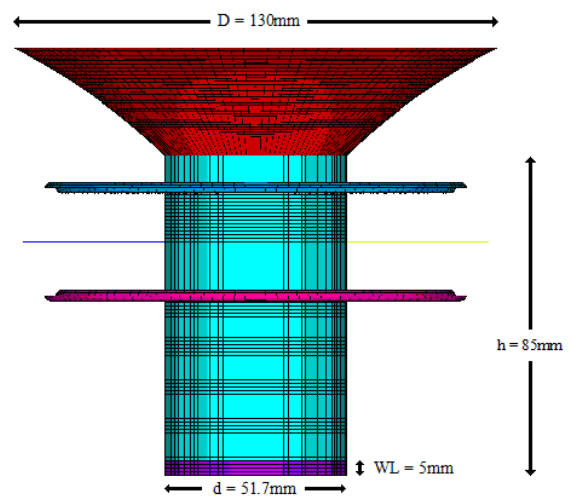


Fig. 8. Moving assembly physical dimensions.

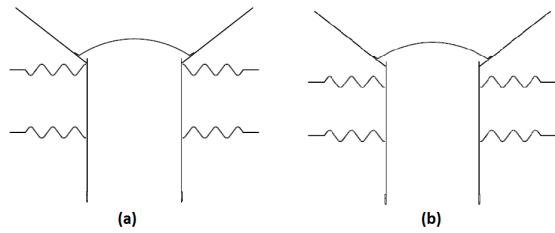


Fig. 9.(a) Symmetrical configuration. (b) Asymmetrical configuration.

Two different types of forces have been considered for each model: balanced and unbalanced. In this model, the force was applied in the voice coil nodes. The balanced force allowed us to adjust the model and evaluate the displacement on y-axis, whereas the unbalanced force lets analyse the risks involved in some configurations. The ideal situation is when the force in y-axis is identical in every voice coil nodes.

But, in a real situation, this does not happen exactly in this way. The unbalanced force tries to respond to these irregularities. One of the origins of these irregularities is the no uniformity of the magnetic field due to the construction tolerances of the air gap. This paper shows the results corresponding to the application of unbalanced forces. This force is depicted in Fig. 10, and it describes a sinusoidal variation along the circumference length of the air gap. Maximum value position is represented by θ (Fig. 11) and its possible values are $\theta=0^\circ$, $\theta=90^\circ$ and $\theta=180^\circ$, covering a wide range of possible situations. Maximum unbalanced force has been considered as a 5% of the magnetic force in each case, calculated as

$$F = Bli \tag{12}$$

In Fig. 11, apart from θ , δ was also defined as the angle between both lead wires. Two different possibilities were studied. First one consists on placing the lead wires with $\delta=30^\circ$ ($+15^\circ$, -15°) and the second one consists on separating them 180° , which means $\delta=180^\circ$. This solution was thought with the aim of achieving an optimal structural equilibrium.

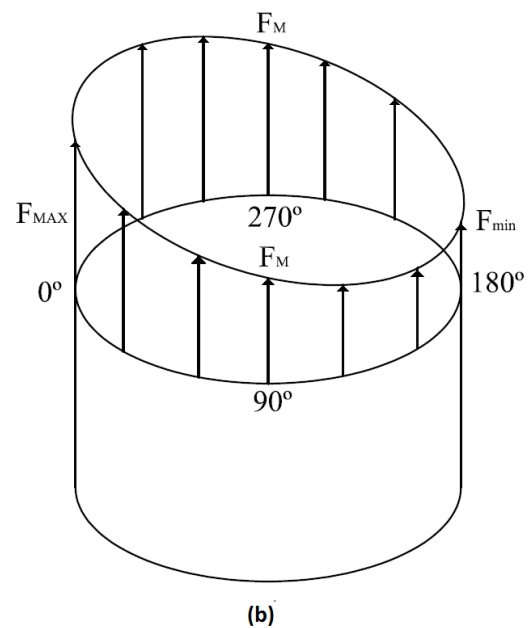
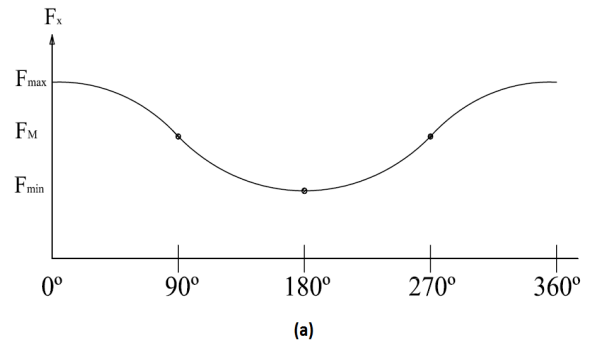


Fig. 10. Scheme of unbalanced forces applied to the model.

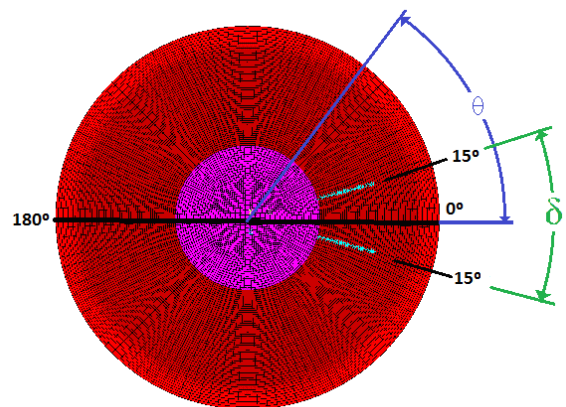


Fig. 11. Lead wires placement for the implemented model.

4. RESULTS

Most representative results are exposed below these lines.

4.1. Modal analysis. Participation factors.

Modal shapes observation provides important information. As an example, in Fig. 12, two modes are shown. Fig. 12(a) shows the main mode, whose movement is in the y-axis (vertical) and it does not present any other component. Fig. 12(b) shows a complex mode characterized by a moving assembly rocking motion.

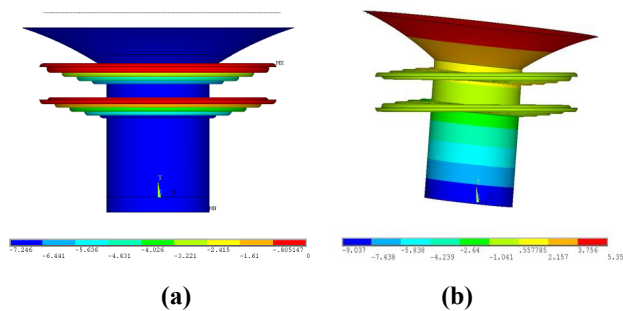


Fig. 12. (a) Moving assembly main mode (b) Rocking motion mode

Fig. 13 depicts the participation factors of modal shapes between 50 Hz and 1 KHz when applying an unbalanced force with $\theta = 0^\circ, 90^\circ, 180^\circ$ when lead wires are placed with $\delta = 30^\circ$.

It can be observed that the mode placed at 52 Hz, where mechanical resonant frequency of the system is located, presents a higher participation factor than other modes for every situation.

This work aims to explain exclusively low frequency issues. For this reason, simulations only show results until 400 Hz.

In Fig. 13, the circled zone has been zoomed so that it can be appreciated that participation factor variation is function of the type of unbalanced forces. The participation factor of this mode is higher when the force presents a maximum at $\theta = 90^\circ$.

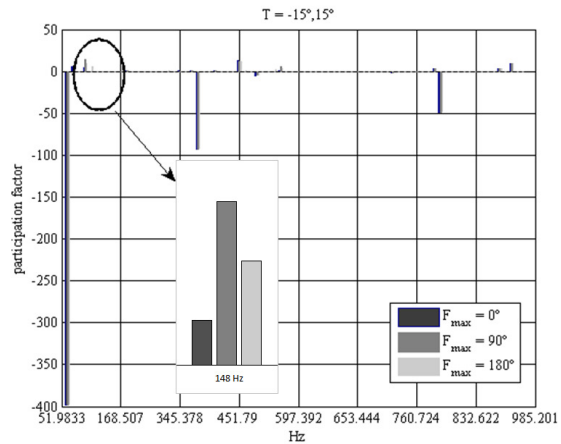


Fig. 13. Most significant participation factors within the range 50Hz -1KHz

Fig. 15 shows a simple analysis, where a maximum displacement in the x-axis, u_x , has been depicted in two different positions shown in Fig. 14. As it can be noticed, position A is the bottom of the former whereas position B is the top of the membrane. Displacements in position A are greater than displacements in position B in the frequency range mentioned before. This simulation was done considering $\theta = 90^\circ$ and $\delta = 30^\circ$.

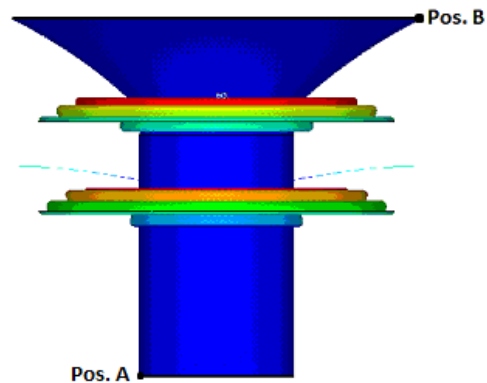


Fig. 14. Lead wires position with $\delta = 180^\circ$. Positions A and B considered to analyse displacements.

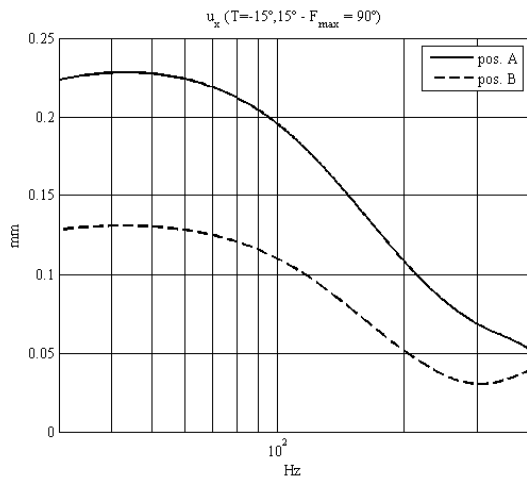


Fig. 15. Comparison between displacements in the x-axis in two different positions.

4.2. Influence of the number of folds in the suspension

4.2.1. Displacement in the y-axis

Fig. 16 shows displacement in the y-axis for a single point in position A when $\delta = 180^\circ$ and $\theta = 90^\circ$. Since sound radiation occurs from 52 Hz, it is possible to conclude that displacement variation in the y-axis is practically negligible.

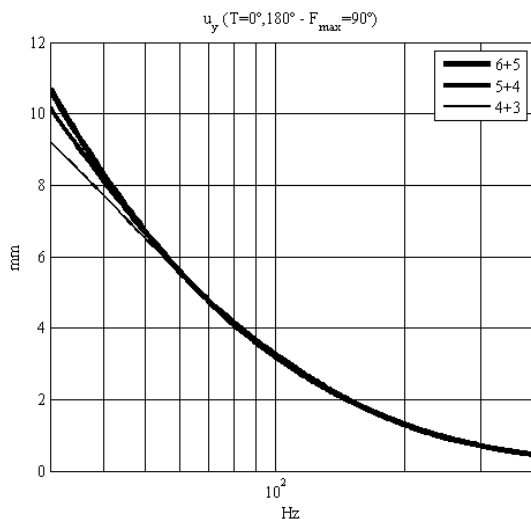


Fig. 16. Effect on the number of folds in the y-axis displacement.

By simple inspection, it is clear that varying the number of folds only has effects on very low frequencies, where

the loudspeaker does not work. From 60 Hz, y-axis displacement is independent of this variable.

4.2.2. Displacement in the x-axis

Fig. 17 shows displacement in the x-axis for two different positions: A and B, where A and B are the same positions explained before. The distance between suspensions is 30 mm and the number of folds in the suspension is the parameter of interest in this case.

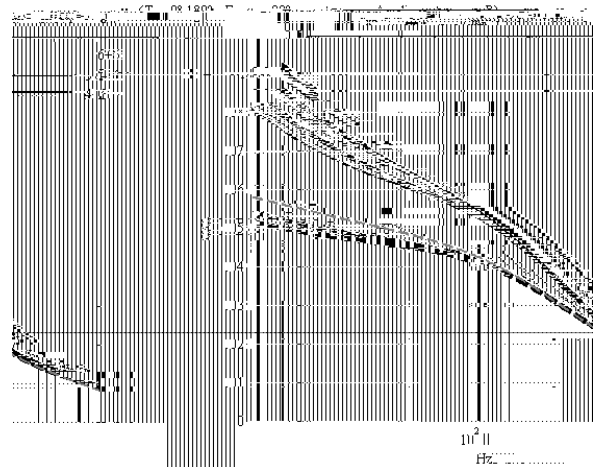


Fig. 17. Maximum displacement in the x-axis when $\delta = 180^\circ$ and $\theta = 90^\circ$

Results show that the most favourable situation is when using a higher number of folds because x-axis displacement is lower. For this reason, 6+5 folds configuration was chosen instead of 5+4 or 4+3. Number before + indicates folds facing up, whereas number after + indicates folds facing down.

4.3. Distance between suspensions

Fig. 18 depicts displacement in the x-axis for a single point in position A, modifying the distance between the suspensions. As it was expected, the greater the distance, the lower the displacement in the x-axis.

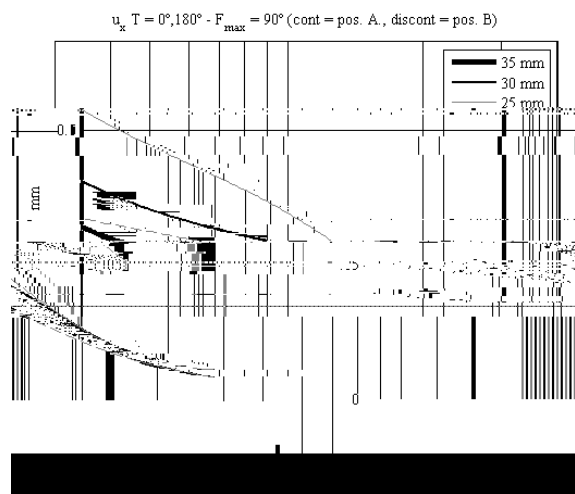


Fig. 18. Effect of distance between suspensions.

4.4. Lead wires location

Fig. 19 compares displacements in the x-axis when $\delta = 30^\circ$ and $\delta = 180^\circ$. Displacements are smaller in the second case (discontinuous lines) so it is possible to assert that this option ($\delta = 180^\circ$) is more stable than the first one ($\delta = 30^\circ$).

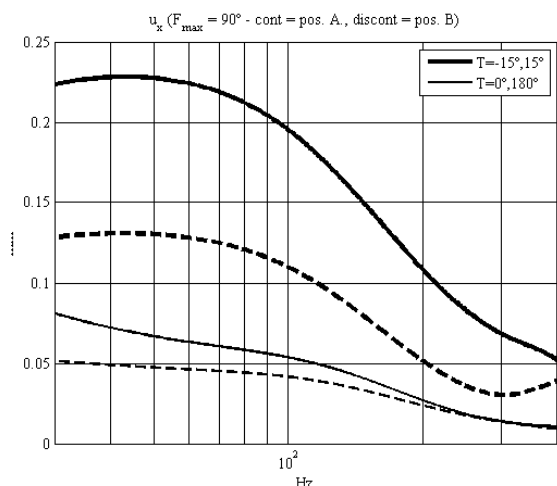


Fig. 19. Displacement in the x-axis varying lead wires location.

4.5. Configuration for double suspension

In this section, the most optimal orientation for double suspension is studied. Fig. 20 shows simulation results for x-axis displacement for a single point placed in position A for two different suspension orientations: symmetrical and asymmetrical, Fig. 9. When $\delta = 30^\circ$

and $\theta = 90^\circ$, the symmetrical presents more stability. This result is also given for other unbalanced forces.

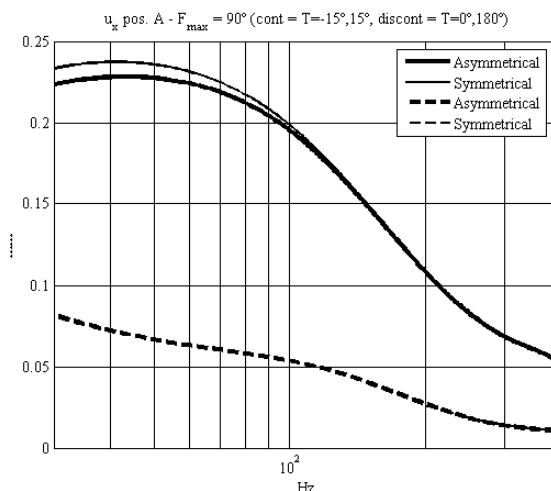


Fig. 20. Displacement in the x-axis for symmetrical and asymmetrical suspension orientation.

When the lead wires are placed with $\delta = 180^\circ$ (discontinuous lines), both discontinuous curves are superposed. This indicates that displacement in the x-axis has nothing to do with suspension orientation.

4.6. Comparison with commercial models

Once studied the theoretical results offered by the numerical model, an experimental driver was built with the following characteristics: suspensions had 6+5 folds and they were placed symmetrically, lead wires were positioned with $\delta = 180^\circ$, and distance between suspensions was 30mm due to constructive limitations.

This experimental driver was compared with 5" and 6"1/2 loudspeakers because the effective surface area S_D is 132cm^2 , which is higher than 5-inch loudspeaker S_D (95cm^2) but slightly smaller than 6"1/2 loudspeaker S_D (140cm^2).

Fig. 21 shows diaphragm displacement measurements corresponding to an excitation voltage of 15V. It can be observed that both commercial loudspeakers are in the nonlinear behaviour zone, whereas the experimental driver is working under perfect linear conditions.

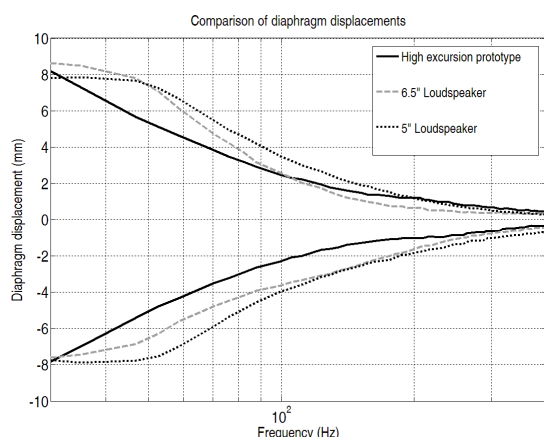


Fig. 21. Diaphragm displacement comparison between the experimental driver and the commercial loudspeakers when applying an input voltage of 15V

Furthermore, SPL measurements were realized at 1m with an excitation voltage that allows each loudspeaker to work in the limit of nonlinearity.

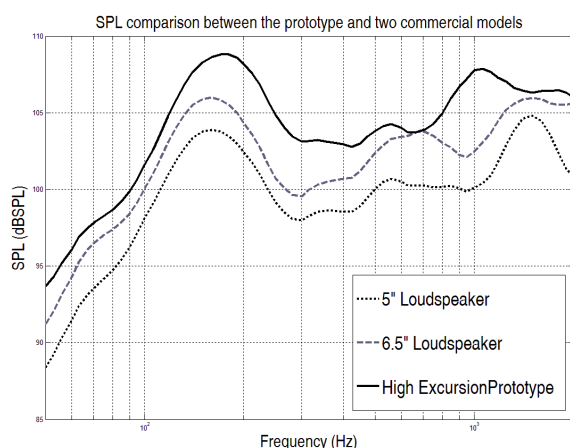


Fig. 22. SPL comparison between proposed experimental driver and two commercial models working in its linear zone limit

Fig. 22 shows that the experimental driver SPL is noticeably higher than the commercial loudspeakers.

5. CONCLUSIONS

A Finite Element Model was implemented to study the structural behaviour of moving assembly in a small size and high excursion loudspeaker. This work fits into the context of a project where one of its goals is to assess the feasibility of implementing a loudspeaker without upper suspension in order to facilitate very important excursions.

To adjust suspension material Young modulus in the numerical model, an experimental driver was built. Knowing its resonant frequency and the moving assembly mass, it was possible to adjust it using an inverse technique.

To determine loss factor, displacement measurements were carried out using Klippel analyser system. Adjustment was completed assuming that the model behaves like a SDOF system.

Once the model was accurately adjusted, it was simulated in order to evaluate the effect of balanced and unbalanced forces.

Results presented showed that number of folds in the suspension is not very important when considering y-axis displacements, but they are important to minimize the x-axis displacement. For this reason, 6+5 fold suspension was chosen when making the experimental driver.

It was also seen that distance between suspensions have little influence in the x-axis displacements, although values are practically insignificant. Therefore, the distance between suspensions was decreased from 35mm to 30 mm. This way, the loudspeaker implementation became more feasible.

Moreover, it was explained how the lead wires location affects the x-axis displacement. The best option is to place them with $\delta = 180^\circ$ because this configuration gives the moving assembly more stability.

Finally, the experimental driver has a higher SPL while it is working in its maximum of linear behaviour zone in comparison with two similar size commercial models.

6. REFERENCES

- [1] D. B. Keele, Jr., "Maximum Efficiency of Direct Radiator Loudspeakers," presented at the 91st convention of the Audio Eng Soc., preprint no. 3193 (Oct. 1991)
- [2] Ronald M. Aarts, "High-Efficiency Low-BI Loudspeakers," J. Audio Eng Soc., Volume 53 Issue 7/8 pp. 579-592 (July 2005)
- [3] Gander, Mark R., "Moving-Coil Loudspeaker Topology as an Indicator of Linear Excursion

Capability”, presented at the 64th AES Convention New York City, preprint no. 1554, November 1979.

[4] Carlson, D.; Frye, K; Keele, Jr., Don. B. (Don); Long, J; Newman, R. J.; Ruhlen, M., “An Important Aspect of Underhung Voice-Coils: a Technical Tribute to Ray Newman”, presented at the 121st AES Convention San Francisco, preprint no. 6911. October 2006

[5] Klippel, W, “Diagnosis and Remedy of Nonlinearities in Electrodynamical Transducers”, presented at the 109th AES Convention Los Angeles, preprint no. 5261, September 2000

[6] Leo L. Beranek, Acoustics. McGraw-Hill, New York, 1954.

[7] O. C. Zienkiewicz, “*El método de los elementos finitos*”, Ed. Reverté, (1982)

[8] *ANSYS theory reference 8.1*, ANSYS Inc, (2003)

[9] Klippel, W, “Assessment of Voice-Coil Peak Displacement X_{max} ,” J. Audio Eng Soc., Volume 51 Issue 5 pp. 307-324 (May 2003)